Available online at www.sciencedirect.com

ScienceDirect

Procedia CIRP 42 (2016) 673 – 678

www.elsevier.com/locate/procedia

18th CIRP Conference on Electro Physical and Chemical Machining (ISEM XVIII)

Structure and Composition of the White Layer in the Wire-EDM Process

F. Klocke[a], L.Hensgen[a]*, A. Klink[a], L. Ehle[b], A. Schwedt[b]

[a] *Laboratory for Machine Tools and Production Engineering of RWTH Aachen University*
[b] *Central Facility for Electron Microscopy of RWTH Aachen University*
* Corresponding author. Tel.: +49-241-80-28175; fax: +49-241-80-22293. *E-mail address:* l.hensgen@wzl.rwth-aachen.de

Abstract

In components under bending load the top layer of the workpiece is strained the most. The properties of this layer are therefore very crucial for the mechanical behavior of the component as a whole. The Wire-EDM process, like every machining process, interacts with this surface layer by thermal material load and modification. The thermal material removal principle in Wire-EDM creates a characteristic rim zone alteration. The process generates especially an outer shell that is known as white layer. Although this layer is generally reducing the mechanical endurance, the precise structure and composition of this layer is unknown. The characteristics of the white layer should affect the mechanical behavior significantly. This motivates a comprehensive analysis of this layer within this paper. Chemical analyses of the rim zone together with TEM-images allow identifying the structural constitution of the microstructure. The influence of local defects and transformations on the workpiece functionality is investigated. For determining the chemical composition of the white layer EDX-maps and conventional EDX-analyses were generated. In addition nanoindentation-based mechanical testing methods measure the local hardness and modulus of elasticity in the white layer. By comparing the measured local hardness and modulus of elasticity of the altered rim zone with an unaffected surface layer the influence of the edge geometry is quantified. The addition of the mentioned analyses allows a complete characterization of the chemical composition and metallurgical constitution in the white layer. These characteristics define mainly the mechanical properties of the white layer. This helps predicting the mechanical behavior of workpieces machined with Wire-EDM, especially for components with high aspect ratios and filigree geometries.

Peer-review under responsibility of the organizing committee of 18th CIRP Conference on Electro Physical and Chemical Machining (ISEM XVIII)

Keywords: Wire-EDM; white layer; heat affected zone; mechanical properties; chemical composition

1. Introduction

The improvements in the process design and generator control of Wire-EDM allows the usage of this manufacturing technology also for mechanical demanding applications. Wire-EDM is applied for example in producing aircraft components or flexure hinges [1],[2]. The resulting stresses in a part under bending load are the highest directly under the surface [3]. Therefore the mechanical durability of the white layer is very crucial for the behavior of the workpiece. The crack initiation for EDMed components is typically localized directly under the surface in the white layer [4]. The characteristics of this layer are determined by the chemical composition and the thermal alteration through the machining process. They are mainly influenced through the high local temperature caused by the electric discharge during the EDM-process [5]. The high temperatures and especially the large temperature gradients result in a rapid quenching of the melted workpiece material [6]. This dependence was motivation for several works focusing on the white layer. First analyses regarding the effect of the white layer on the mechanical behavior of the workpiece were performed by König and Siegel [7]. A general characterization of the Wire-EDM trim cut operations and the influences on the white layer was performed by Huang, Liao and Hsue [8]. Aspinwall et. al. as well as Klink, Guo and Klocke investigated the characteristics of the resolidified layer for W-EDM. Both groups couldn't find an increased hardness of the white layer in microhardness measurements [9],[10]. Cusanelli et al., Ekmekci and Lee et. al. investigated the white layer in S-EDM. Cusanelli et al. characterized the metallurgy of the white layer in S-EDM [11]. The recast layer was partly amorphous and partly crystalline. Ekmerkci found an

Peer-review under responsibility of the organizing committee of 18th CIRP Conference on Electro Physical and Chemical Machining (ISEM XVIII)
doi:10.1016/j.procir.2016.02.300

independency of the residual stress distribution in the workpiece from dielectric and tool electrode [12]. Lee et. al. correlated the process parameters with the crack density in the recast layer for EDM-drilling [13]. Poulachon et. al. performed similar work for turning. They found a reduction of white layer thickness for increased parent material hardness [14]. But all these scientific papers excluded the mechanical characteristics of the white layer itself. For these reasons the chemical composition and metallurgical condition together with the local hardness and modulus of elasticity of the white layer will be characterized for the first time in this paper. This should deepen the knowledge about the mechanical behavior of this layer.

Nomenclature

α	angle between the faces of the indenter
δ_r	depth below surface (µm)
E	Young's modulus (GPa)
E_r	reduced elastic modulus (N/µm^2)
EBSD	electron backscatter diffraction
EFTEM	energy-filtered TEM
EPMA	electron probe microanalyzer
FIB	focused ion beam technic
GIXD	grazing incidence X-ray diffraction
H	hardness (kN/mm^2; HV 30)
HAZ	heat affected zone
ν	Poisson's ratio
S-EDM	sinking electro discharge machining
STEM	scanning TEM
TC	trim cut
TEM	transmission electron microscopy
W-EDM	wire electro discharge machining
WL	white layer
XRD	X-ray diffraction

2. Experimental Setup

In order to analyze the composition and characteristics of the white layer, steel workpieces were processed using Wire-EDM. All experimental work was carried out on a Sodick AP200L W-EDM machine tool. The machine tool uses CH-based dielectrics, in this case the oelheld IonoFil 2776. The diameter of the chosen uncoated brass wire is d = 0.2 mm. The powder metallurgical cold work tool steel Vanadis 4 Extra (X140 CrMoV5-4-4 PM) was used as workpiece material. This tool steel combines high strength with good ductility. The composition of the steel is given in Table 1.

Table 1. Alloy composition of X140 CrMoV5-4-4 PM [15].

element	Fe	C	Si	Mn	Cr	Mo	V
chemical composition Wt %	85.9	1.4	0.4	0.4	4.7	3.5	3.7

For achieving the best surface quality nine trim cuts were chosen from the machining data base, see [16]. The achieved surface roughness is around Ra = 0.09 µm. The resulting white layer thickness is δ_r = 0.2 µm. For measuring the local hardness and modulus of elasticity the machining technology was adapted. Through this adaption the resulting white layer thickness was δ_r = 3 µm. This ensures a reliable measuring of the characteristics of the layer. Therefor the trim cuts 3 to 5 were omitted. This results in a relatively thick white layer together with a smooth and flat surface. The energy-dispersive X-ray spectroscopy (EDX) analysis and the EDX-maps were generated in a JSM7000F scanning electron microscope by JEOL equipped with Schottky field-emission gun and a combined EDX/EBSD-system by EDAX-TSL consisting of a Si(Li)-EDX detector and a "Hikari" EBSD camera.

For analyzing the local metallurgical structure of the white layer a thin FIB-lamella was fabricated using the focused-ion-beam technic (FIB). The transmission electron microscopy (TEM) characterizations were performed with a Tecnai F20 transmission electron microscope equipped with a field emission gun (FEG). The energy-filtered (EF)TEM images were acquired with a Gatan CCD camera. The extraction voltage of the electrons was 200 kV. The software used to acquire and evaluate the images was ES Vision for scanning (S)TEM images and EDX data and Gatan Digital Micrograph for EFTEM images.

For measuring the local mechanical characteristics of the white layer an impact of the parent material should be avoided. The principle of the nanoindentation-analysis is similar to the principle of microhardness measurements. But the testing force of the indents is around the factor 100 lower compared to microhardness measurements [17]. Therefore the local resolution of the hardness-analysis is significantly increased. For microhardness testing the ISO-standard 4516 defines requirements for the layer thickness and surface quality [18]. The standard recommends a polished surface quality and a layer thickness greater than 1.4 times the indentation diagonal if the layer is analyzed in the cross section. In order to achieve these requirements the machining technology was adjusted and the cross section was polished. The reduced geometrical stiffness at the edge caused through the lack of support from surrounding material could interact with the effect of the white layer. For minimizing this interaction a nickel support layer was fabricated on top of the surface using galvanic deposition. To quantify the remaining deviation in hardness and modulus of elasticity a specimen with the same geometry but without a white layer was machined using grinding and polishing. The two specimens were etched in order to identify the white layer more easily. Afterwards they were polished again to achieve a smooth surface for the indents of the hardness measurement. Picture 1 exemplarily shows the rim zone of one specimen after etching and after final polishing and nanoindentation analysis.

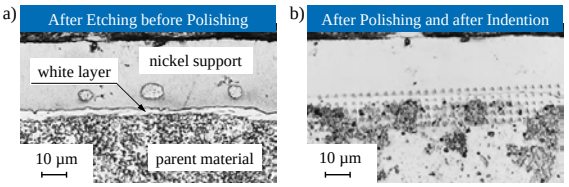

Fig. 1. Analyzed rim zone (a) prior to the final polishing and (b) after polishing and nanoindentation.

The two images illustrate the difference in visibility of the white layer and vice versa the reduced surface quality in the etched cross section. The diamond indenter was a so called “Berkovich”-indenter formed as a three-sided pyramid with an angle between faces of $\alpha = 135°$ [19]. The used testing and analyzing system was a Hysitron TI-900 TriboIndenter.

3. Results

For understanding the mechanical characteristics of the white layer it is necessary to identify the metallurgical structure and chemical composition. In a first step the chemical composition was investigated. Determining the distribution of elements in the white layer allows defining the homogeneity and degree of contamination with elements from parent material and wire electrode. Figure 2 illustrates the characteristic element distribution of a surface machined with nine trim cuts in an EDX-map.

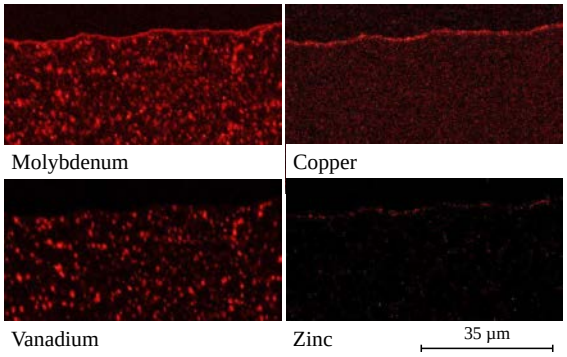

Fig. 2. Chemical element distribution in the white layer and rim zone.

The EDX-map visualizes the counts of a certain element over the position in the rim zone. More counts of an element at one position result in a brighter corresponding spot in the map. Quantifying the total chemical composition of the rim zone is not possible. Overcoming these restrictions five conventional EDX-analyses of the white layer were conducted. Table 2 shows the resulting average composition.

Table 2. Average chemical composition of the white layer.

element	Fe	Cu	Cr	Zn	Mo	V
chemical composition Wt%	87.1	3.2	2.0	2.4	3.1	1.8

The parent material contains molybdenum and vanadium as carbides, visualized as bright spots in the EDX-map. The white layer contains copper and zinc coming from the wire electrode. The amount of zinc is reduced compared to copper. This corresponds with element distribution in the brass alloy (CuZn37) of the wire electrode [20]. The molybdenum coming from the carbides of the parent material was mixed and alloyed in the white layer. Vanadium was just locally found in the white layer therefore the average composition shows just a small amount of vanadium. The same behavior was observed for chromium, not depicted.

The reason for this behavior can be found in the thermo-physical characteristics of the elements. Iron and molybdenum require almost the same quantity of thermal energy for melting whereas the energy for vanadium needs to be increased with the factor 1.3 [21], [22]. Therefore vanadium stays localized, whereas molybdenum was mixed into the white layer and significantly influences the mechanical characteristics of the resolidified layer.

The alloyed molybdenum and copper increase the hardness of the steel [3]. Molybdenum additionally improves the strength of the alloy [23]. The content of zinc has no significant influence on the mechanical properties. In general it reduces ductility only combined with a high percentage of silicon [3]. All the presented chemical alterations of the white layer increase the hardness of the material. This would be enhanced through the possible deposition of carbon from the dielectric. Unfortunately the atomic mass of carbon is not high enough for reliable EDX-characterizations.

Beside the chemical composition the thermal alteration modifies the metallurgical structure of the white layer. A similar white layer was sketchy investigated in previous work [24]. Figure 3 exemplarily shows an EBSD-image-quality-map of the rim zone. The image-quality-map illustrates the crystallinity of the rim zone.

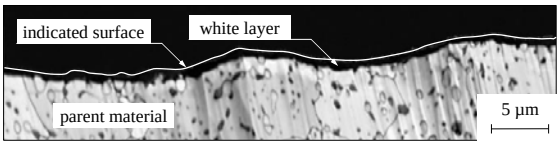

Fig. 3. Rim zone of nine trim cuts visualized with EBSD [22].

The picture demonstrates that the material in the resolidified layer was not crystalline enough to create a signal in the EBSD-analysis. Defining the metallurgy in the white layer more dependably is a key objective of this investigation. For identifying the actual metallurgical state of the white layer TEM-analyses were conducted. Figure 4 depicts the EDMed surface analyzed using STEM.

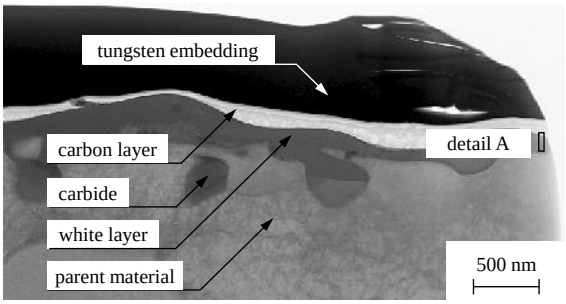

Fig. 4. Prepared FIB-lamella with carbon and tungsten support layers.

For protection reasons the surface was coated with carbon and tungsten prior to the FIB-preparation. The tungsten layer shields the white layer from the ion beam. The deposed tungsten is in crystalline form. Therefore the electron beam analyzing the white layer would interact with this tungsten, a profound analysis of the resolidified material is not possible. To overcome this limitation a fine carbon layer was deposed between. This layer is fully amorphous and does not influence the investigation of the white layer. The recast layer has an average thickness of around $\delta_r = 0.2$ µm. Figure 5 illustrates "detail A" from Fig. 4 with much higher magnification using the EFTEM method, allowing to identify the microstructure. The FIB-lamella gets thinner from left to right. A thin lamella results in a improved image quality. Therefore the detailed analysis was conducted in the very right part of the lamella.

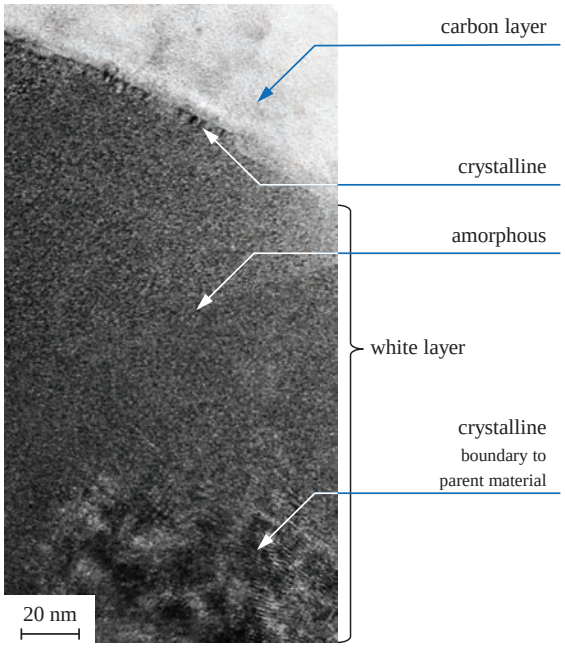

Fig. 5. Detail A: Close-up on the white layer using EFTEM.

Using diffraction patterns the crystallinity of the white layer was identified and localized in the picture. The area in the middle of the picture that appears unstructured and tarnished is fully amorphous. The part of the resolidified material that is located close to the parent material is of crystalline microstructure. The depth of crystalline parts in the white layer is non-uniform. In the very left part of the picture areas of the same depth can be observed that are fully amorphous. Directly below the interface between white layer and carbon layer the microstructure is locally (thickness below $\delta_r = 4$ nm) crystalline. Identifying the reasons for this crystallinity need further investigation. One explanation could be found in the preparation process. During the carbon deposition recrystallization could be induced by the slightly increased temperature.

The general comparison with the white layer observed by Cusanelli et. al. shows similarities of the structures [12]. This is noticeable when considering that the difference in layer thickness, discharge energy and exposure time is huge (Cusanelli et al. examined a S-EDM process). This corresponds with the results of Huang et. al. [25]. The amorphous layer indicates a huge quenching of this material. A very hard and brittle mechanical characteristic could be expected. In generally the hardness and brittleness together with a reduced ductility can be correlated [3]. This motivates the investigation of the local hardness and modulus of elasticity in the white layer.

In order to investigate the hardness of the white layer in detail nanoindentation analyses were conducted. Similar analyses were used from Kompella et. al. for the characterization of white layers in grinding [25]. Chen et. al. applied the nanoindentation for the characterization of thermal alterations in machining cast iron [27].

Due to the minimum layer-thickness for the nanoindentation, the actual white layer thickness was increased by the technology adjustments. The achieved layer thickness of $\delta_r = 3$ µm exceeds the requirements [28]. Figure 6 illustrates the measured hardness profile of white layer and parent material. The picture on the right shows the corresponding rim zone before polishing and the final indentation analysis.

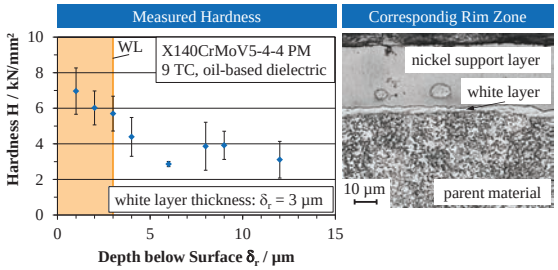

Fig. 6. Local hardness in white layer and parent material.

The representative white layer thickness is given as orange field in the diagram. The distance of each indent from the actual surface was linked to the hardness value itself. In total the depicted profile consists of 93 single indentation analyses.

The hardness value of the parent material is around $H = 3.5$ kN/mm^2. Due to the specific nanoindentation measurement using a "Berkovich"-indenter the hardness is given as a pressure. Through complementary Vickers-hardness measurements the values can be classified. The according Vickers-hardness of the parent material is $H = 219.9$ HV 30. Basically the hardness decreases from surface to parent material. The maximum hardness is reached close to the surface of the resolidified layer with a value of $H = 7$ kN/mm^2. The hardness of the nickel support layer can be quantified as $H = 4.9$ kN/mm^2. So the support will not increase the measured hardness of the recast layer. Inside the white layer the hardness increases from parent material to surface. One reason for this behavior can be found in the higher concentration of copper and possibly carbon directly below the surface. A second cause is the increased quenching

of the top layers caused by the greater heat flux into the dielectric.

Klink et. al. used micro-hardness measurements performed on the machined surface layer (top view with a WL-thickness of $\delta_r < 1$ µm) [10]. Therefore their results were significantly influenced through surface roughness (for indentation depth of 0.5 µm) and the characteristics of parent material (for a depth of 3.5 µm), regarding ISO 4516 [18]. By measuring the hardness in the cross-section of the workpiece the restrictions Klink et. al. observed in their investigation were avoided.

Possibly the determined hardness was influenced by the reduced support of surrounding material right at the edge of the workpiece. For quantifying this possible deviation the descripted measurement were also applied to a surface without thermal alteration due to pure polishing. The resulting local hardness measurements are shown in Figure 7.

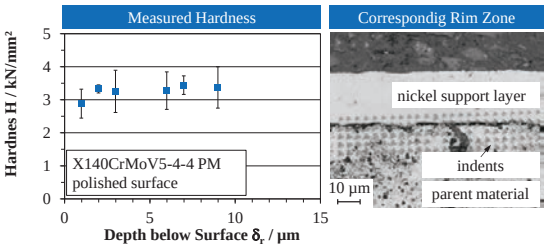

Fig. 7. Hardness profile of the surface layer without heat-affected zone.

This hardness profile consists of 66 indentations. The hardness of the parent material is equal to the values of figure 6. The adhesion of the nickel support layer was slightly reduced on this surface, visible as dark gap between support layer and parent material in the light microscope image. This resulted in a somewhat decreased hardness in the first $\delta_r = 1$ µm. Despite this effect no change in the hardness profile as function of depth below surface is visible. The nickel support layer minimizes geometrical effects caused by the edge of the workpiece. Therefore the achieved values of the hardness in the white layer are reliable and not deviated through geometrical effects.

In addition to the local hardness tests the nanoindentation analysis is also capable of determining the local modulus of elasticity. In the indentation process subsequent to the increasing of indentation force the load will be constantly reduced. During this reduction of load the workpiece material in the first part springs back elastically. The gradient of the displacement- unloading curve in this section can be correlated with the reduced elastic modulus E_r. Knowing the Poisson's ratio ν of the analyzed material the Young's modulus E can be calculated [28]. Using the Poisson's ratio of steel $\nu = 0.27$ the Young's modulus of the rim zone was determined. Therefore the analyses of elastic modulus are derived from the local hardness measurements. The database for this analysis is the same number of indents as for the local hardness. The resulting elastic modulus for the altered and the unaffected surface layer is depicted in Figure 8.

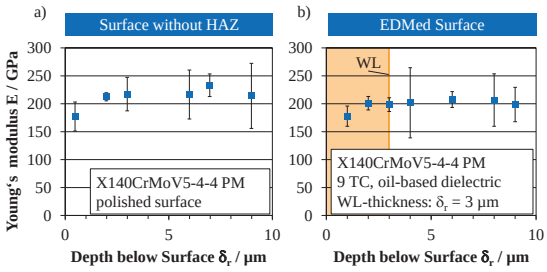

Fig. 8. Comparison of Young's modulus: (a) unaffected surface, (b) with white layer.

In general the Young's modulus is the same for both surfaces. It is around the value of the modulus of steel E = 210 GPa. Only the values directly under the surface are slightly reduced, compared to parent material. The depth of the area of reduced elastic modulus is around $\delta_r = 1.5$ µm. This behavior can be found in both surfaces. An influence from the white layer can be neglected. The reason for the slightly reduced elastic modulus at the boundary to the nickel support layer can be found in the interaction of the different materials and the mechanical properties of nickel. The measured Young's modulus was just E = 175 GPa. This measured modulus of elasticity is a bit smaller compared to the value of the literature E = 186 GPa [29]. But both values are significantly below the modulus of steel. Therefore the first row of indents is not fully supported from steel, but partly from nickel. The measured elastic modulus is slightly reduced compared to parent material.

Altogether the white layer does not affect the modulus of elasticity of the workpiece material. Both the contamination with material from tool electrode, dielectric and carbides and the heavy quenching of the amorphous material didn't influence the Young's modulus.

4. Conclusion and Outlook

The task for this investigation was to characterize the chemical composition, structure and mechanical properties of the white layer resulting from a Wire-EDM fine machining process. The following results were achieved:

- In a first step the chemical composition of the white layer was analyzed. The recast layer contains elements from the wire electrode (copper and zinc) and allocated molybdenum from carbides of the molten parent material. Vanadium and chromium were not allocated and mixed into the white layer.
- In a second step the metallurgical state of the recast layer was determined using TEM analyses. The white layer is mainly of amorphous microstructure. At the boundary to parent material crystalline structures spread into the amorphous regions. In the first $\delta_r = 4$ nm below the surface the material was of crystalline microstructure, possibly because of the deposition process of the carbon layer.

- The third step was to quantify the local hardness in the white layer and in the area below this layer. The hardness of the recast layer is significantly increased. The hardness nearly doubles in the white layer compared to parent material. Effects from the geometry of workpiece edge could be negated.
- The last analysis focused on the modulus of elasticity in the white layer in comparison with an unaffected surface. The Young's modulus was not altered through the characteristics of the white layer. A small deviation close to the surface was caused by the nickel support layer.

Some aspects of the recast layer characteristics could not be evaluated. So in future work the contamination with carbon and the residual stress distribution of the white layer should be investigated. Carbon and molybdenum have great impact on the mechanical properties of a steel component [3]. Using analyzing technologies like the electron probe micro-analyzer (EPMA) the chemical portion of the element carbon (small atomic mass) can be quantized for the white layer. The tensile residual stress is stated as the main reason for cracks under bending load [6]. Because of the small depth of the residual stress zone for the analyzed trim cut operation the stresses are not detectable with conventional XRD-measurements [16]. The grazing incidence X-ray (GIXD) diffraction is able to overcome this limitation because of the flat attack angle of the X-rays. As a result the excitation volume reaches far fewer in the depth of workpiece. A characterization of thin residual stress zones will be possible. The stress profile in the white layer and directly below this layer can be specified.

Acknowledgements

This study was conducted with financial support from the German Research Foundation (DFG) by the Collaborative Research Center SFB/TRR 136 "Process Signatures" and (Bremen, Aachen, Oklahoma), subprojects C02 and F02, and the project „Grundlegende Untersuchungen zu stoffschlüssigen Gelenken mit Einsatz in parallelkinematischen Mikromanipulatoren", hereby gratefully acknowledged.

References

[1] Welling D. Results of Surface Integrity and Fatigue Study of Wire-EDM Compared to Broaching and Grinding for Demanding Jet Engine Components Made of Inconel 718. Procedia CIRP 13. 2014. 339–344.
[2] Klocke F, Hensgen L, Klink A, Corves B, Schoenen D, Hüsing M. High precision flexure hinges – functional-based machining optimization EUSPEN 14 (14). 2014. 79–82.
[3] Dubbel H, Grote K, Feldhusen J. Dubbel: Taschenbuch für den Maschinenbau. 24th ed. Springer. Berlin, Heidelberg. 2014.
[4] Fredriksson G, Bergström J, Hogmark S. Fatigue Resistance and Surface Properties of EDMed Cold Work Tool Steels. On the International Conference on Tooling 4. 1996.
[5] Kunieda M, Lauwers B, Rajurkar K, Schumacher B. Advancing EDM through Fundamental Insight into the Process. CIRP Annals - Manufacturing Technology 54 (2). 2005. 64–87.
[6] Klocke, F., König, W. (Eds.). 2007. Fertigungsverfahren: Abtragen, Generieren und Lasermaterialbearbeitung. 4th ed. Springer. Berlin, Heidelberg, New York. XXVII, 390 S.
[7] König W, Siegel R. Funkenerosives Feinstschneiden: Randzonenausbildung und Dauerfestigkeit. 1993.
[8] Huang J, Liao Y, Hsue W. Determination of finish-cutting operation number and machining-parameters setting in wire electrical discharge machining. Journal of Materials Processing Technology (87). 1997. 69–81.
[9] Aspinwall D, Soo S, Berrisford A, Walder G. Workpiece surface roughness and integrity after WEDM of Ti–6Al–4V and Inconel 718 using minimum damage generator technology. CIRP Annals - Manufacturing Technology. 2008.
[10] Klink A, Guo Y, Klocke F. Surface integrity evolution of powder metallurgical tool steel by main cut and finishing trim cuts in wire-EDM. Conference on Surface Integrity (CSI). 2011.
[11] Cusanelli G, Hessler-Wyser A, Bobard F, Demellayer R, Perez R, Flükiger R. Microstructure at submicron scale of the white layer produced by EDM technique. Journal of Materials Processing Technology 149 (1-3). 2004. 289–295.
[12] Ekmekci B. Residual stresses and white layer in electric discharge machining (EDM). Applied Surface Science 253 (23). 2007. 9234–9240.
[13] Lee H, Hsu F, Tai T. Study of surface integrity using the small area EDM process with a copper–tungsten electrode. Materials Science and Engineering: A 364 (1-2). 2004. 346–356.
[14] Poulachon G, Albert A, Schluraff M, Jawahir I. An experimental investigation of work material microstructure effects on white layer formation in PCBN hard turning. International Journal of Machine Tools and Manufacture 45 (2). 2005. 211–218.
[15] Böhler-Uddeholm Deutschland GmbH. 2013. UDDEHOLM VANADIS®4 EXTRA. http://www.uddeholm.de/german/files/downloads/vanadis4_extr-ger_p_0808_e4%281%29.pdf. Accessed 6 August 2013.
[16] Klocke F, Hensgen L, Klink A, Mayer J, Schwedt A. EBSD-Analyse of Flexure Hinges Surface Integrity Evolution via Wire-EDM Main and Trim Cut Technologies. 2nd CIRP Conference on Surface Integrity (CSI) Procedia CIRP (13). 2014. 237–242
[17] Oliver W, Pharr G. An improved technique for determining hardness and elastic modulus using load and displacement sensing indentation experiments. Journal of Materials Research Vol. 7 (6). 1992.
[18] Deutsches Institut für Normung e.V. 2002. Metallische und andere anorganische Überzüge Mikrohärteprüfungen nach Vickers und Knoop. Beuth. Berlin ICS 25.220.40; 25.220.99. Accessed 21 August 2015. 18 pp.
[19] Fischer-Cripps AC. Nanoindentation Testing. Springer. 18 pp. 2011.
[20] Berkenhoff GmbH. Montag, 2013. topas plus: Hochleistungsdrähte für mehr Schneidleistung und Präzision. Accessed 1 August 2013.
[21] Lide DR. CRC Handbook of Chemistry and Physics. 85th ed ed. CRC. Boca Raton, FL, 2005. 2005.
[22] Takahashi Y, Nakamura J, Smith J. Laser-flash calorimetry: Heat capacity of vanadium from 80 to 1000 K. The Journal of Chemical Thermodynamics 14 (10). 1982. 977–982.
[23] Rathore S, Salve M, Dabhade V. Effect of molybdenum addition on the mechanical properties of sinter-forged Fe–Cu–C alloys. Journal of Alloys and Compounds 649. 2015. 988–995.
[24] Klocke F, Hensgen L, Klink A, Mayer J, Schwedt A. Electron Backscatter Diffraction Analysis of Wire-EDMed Surfaces: A new way to identify the metallurgical conditions in process induced rim zones. International Conference on Precision Engineering. 2014. 31–35.
[25] Huang C, Hsu F, Yao S. Microstructure analysis of the martensitic stainless steel surface fine-cut by the wire electrode discharge machining (WEDM). Materials Science and Engineering. 2004.
[26] Kompella S, Moylan S, Chandrasekar S. Mechanical properties of thin surface layers affected by material removal processes. Surface and Coatings Technology 146-147. 2001. 384–390.
[27] Chen L, Zhou J, Bushlya V, Stahl J. Influences of Micro Mechanical Property and Microstructure on Performance of Machining High Chromium White Cast Iron with cBN Tools. Procedia CIRP 31. 2015. 172–178.
[28] Kaupp G. Atomic force microscopy, scanning nearfield optical microscopy and nanoscratching: Application to rough and natural surfaces. Springer-Verlag. Berlin. 301 pp. 2006.
[29] Ledbetter H. Low-temperature magnetic-elastic anomalies in fcc Fe-Cr-Ni alloys. Physica B: Condensed Matter 161 (1-3). 1990. 91–95.